2011 American Control Conference
on O'Farrell Street, San Francisco, CA, USA
June 29 - July 01, 2011

Fundamental Limits in Combine Harvester Header Height Control

Yangmin Xie, *Member*, *IEEE*, Andrew G. Alleyne, *Senior Member*, *IEEE,*
Ashley Greer and Dustin Deneault

***Abstract* — This paper investigates fundamental performance limitations in the control of a combine harvester's header height control system. Utilizing standard frequency domain analysis tools, we are able to demonstrate closed-loop bandwidth limitations that stem from specific system design configurations. There are two primary sub-system characteristics that influence the available bandwidth by affecting the open loop transfer function. The first sub-system is the mechanical configuration of the combine and header while the second sub-system is the electro-hydraulic actuation for the header. The mechanical combine + header sub-system results in an input-output representation that is both under-actuated and has a non-collocated sensor/actuator pair. The electro-hydraulic sub-system introduces a significant time delay. In combination they each reinforce the effect of the other thereby exacerbating the overall system limitation. Simulation and experimental results are provided to validate the existence of these performance limiting sub-systems. Additionally, the overall effect of the system limitations is presented.**

I. Introduction

With the world population increasing over the next several decades, agriculture will be called upon to provide greater yields in food production with relatively little increase in land usage. Therefore, it is imperative that efficiencies associated with automation become part of the overall solution. One key aspect is the machinery used to perform the agricultural tasks; in particular, the combine harvester systems responsible for extracting the crops from the field. The header height control problem under study is motivated by the interest in improving the efficiency and productivity of the harvesting process; specifically, to increase the harvest yield and decrease the total harvest time

The header height control problem is a long standing issue in the combine harvester industry. It has been estimated that approximately 75% of the crop losses occur at the header [1] and a significant portion of the header loss is caused by improper setting of the header height. Fig. 1 shows a schematic of a combine harvester system operating in the vertical plane. The header height is defined as the distance between the header tip and ground. By raising or lowering the header with an actuator, usually hydraulic, the header height can be adjusted. If the header height is too large, there is a reduction in harvest yield since much of the viable crop will be left un-harvested. Conversely, if the header height is maintained at too low a level, equipment damage or operator fatigue will result.

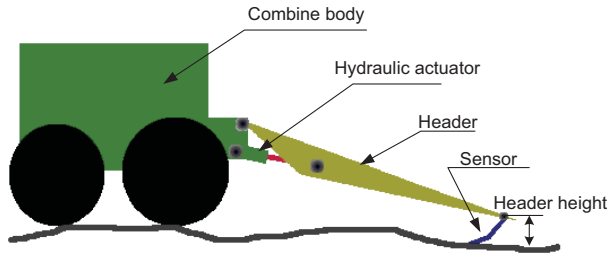

Fig. 1 Combine system

While relevant, this control problem has received relatively little attention from the research community. The common feedback system for the header height control has the structure as Fig. 2. Early approaches were proportional-type controllers with an input dead zone operating around the set-point [2]. One of the few recent investigations to utilize modern control techniques introduced a Linear Quadratic Gaussian (LQG) controller to automatically track changing terrain shapes [3]. Another reduced order state feedback controller was proposed by using a sky hook damper to simplify an optimal full state feedback controller and obtain the output disturbance rejection ability [4]. The feedback control in [3] and [4] works well in simulation at low frequencies: below 1 Hz. Field tests, such as those shown in Section V, illustrate that the achievable bandwidth of a header height control system is much lower in practice.

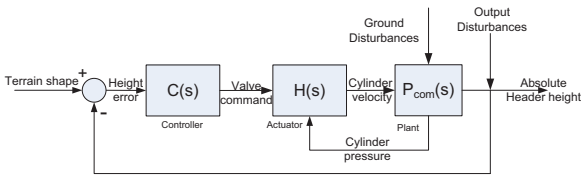

Fig. 2 Schematic of feedback header height control

The rest of paper is organized as follows. Section II introduces the models for the combine system shown in Fig. 1 and Fig. 2. Section III validates the models. Section IV presents an analysis for the performance limitation. Section V complements the analysis by both experiment and simulation. A conclusion provides a summary and offers insight as to possible remedies that could be undertaken.

II. System Modeling

A. Mechanical Sub-System Modeling

The combine system is simplified as the planar multi-body system shown in Fig. 3 and Fig. 4. As such, it contains two

Y. Xie (xie3@illinois.edu) and A. G. Alleyne (alleyne@illinois.edu) are with the Mechanical Science and Engineering Department at the University of Illinois at Urbana-Champaign, Urbana, IL 61801 USA (phone: 217-244-9993; fax: 217-244-6534).

A. Greer (GreerAshleyE@johndeere.com) and D. Deneault (deneaultdustind@johndeere.com) are in the John Deere Company. Champaign, IL 61820-7484

rigid bodies: the combine body and the header, and there are three DOFS with one actuator amounted between the header and the combine body. The active DOF is the header rotation around the attach point A on the combine body. The two passive DOFs are the combine body rotation and vertical translation relative to the center of gravity. The output sensor is installed on the header tip to measure the header height with respect to the ground. Therefore the sensor is non-collocated with the actuator yet is influenced by all 3 DOFs.

In this combine system, flow control valves are used to lift and lower the header. Therefore, the control input to the mechanical system can be assumed to be the velocity of the hydraulic cylinder $\dot{l}_c$. Fig. 3 and Fig. 4 illustrate both the rigid body dynamic analysis and the internally generated forces (F_{Ax}, F_{Az}, F_l) for the combine body and header, respectively. Eqs. (1) through (9) present geometric relationships between the system variables defined in Fig. 3 and Fig. 4. Eqs. (10) through (12) represent force balances by which the three primary dynamic Equations can be represented. Eqs. (13) through (16) represent relationships among forces, motion of bodies and exteral disturbances. Table 1 gives the nomenclature for the variable presented in Eqs. (1) – (16) along with values representative of an actual combine. Exact manufacturer values could not be made available. However these are sufficiently accurate to make subsequent analysis valid.

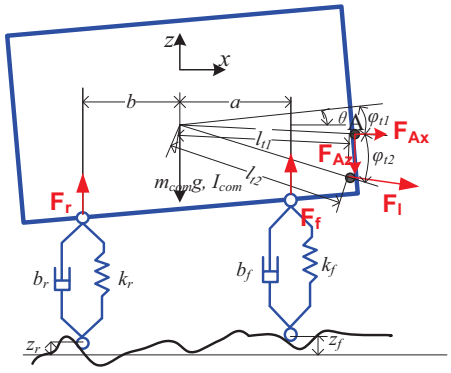

Fig. 3. Force analysis for combine body

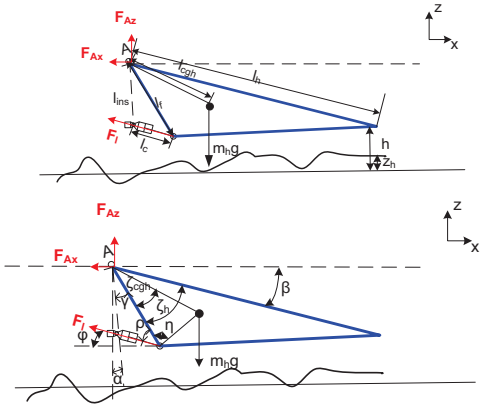

Fig. 4. Force analysis for header

To maintain a desired header height, the absolute header height h in Fig. 4 should track the varying ground profile z_h by controlling the cylinder velocity $\dot{l}_c$. To obtain the open-loop transfer function from z_h (the tracking reference) to h (absolute header height), Eqs. (1) – (16) are linearized about an equilibrium point (Table II). The kinematic relationships in Eqs. (1) – (9) are linearized about a given operating point, using small angle approximations where appropriate. Using the data from Table I and Table II, the resulting dynamic can be represented by Eqs. (17) – (19).

Kinematics

$$
\begin{cases}
l_c^2 = l_{ins}^2 + l_f^2 - 2l_{ins}l_f\cos\gamma & (1)\\
l_{ins}^2 = l_c^2 + l_f^2 - 2l_c l_f\cos\rho & (2)\\
\alpha+\gamma+\zeta_h+\beta=\pi/2 & (3)\\
\zeta_h+\beta-\rho=\varphi & (4)\\
x_A = l_{t1}\cos(\varphi_{t1}-\theta) & (5)\\
z_A = v - l_{t1}\sin(\varphi_{t1}-\theta) & (6)\\
x_{cgh} = x_A + l_{cgh}\cos(\beta+\zeta_h-\zeta_{cgh}) & (7)\\
z_{cgh} = z_A - l_{cgh}\sin(\beta+\zeta_h-\zeta_{cgh}) & (8)\\
h = -l_h\sin\beta + z_A + h_0 & (9)\\
\alpha-\theta+\dfrac{\pi}{2}=\alpha_0 & (10)
\end{cases}
$$

Dynamics

$$
\begin{cases}
I_h\ddot{\beta} = m_h g l_{cgh}\cos(\beta+\zeta_h-\zeta_{cgh}) - F_l l_f\sin(\rho) & (10)\\
m_{com}\ddot{v} = -F_{Az} + F_l\sin\varphi - m_{com}g + F_f + F_r & (11)\\
I_{com}\ddot{\theta} = F_f a - F_r b - F_l l_{t2}\sin(-\varphi+\varphi_{t2}-\theta) \\
\quad + F_{Ax}l_{t1}\sin(\varphi_{t1}-\theta) - F_{Az}l_{t1}\cos(\varphi_{t1}-\theta) & (12)
\end{cases}
$$

Forces

$$
\begin{cases}
F_{Ax} = -m_h\ddot{x}_{cgh} + F_l\cos\varphi & (13)\\
F_{Az} = m_h\ddot{y}_{cgh} + F_l\sin\varphi + m_h g & (14)\\
F_f = -k_f(a\theta - z_f + v) - b_f(a\dot{\theta} - \dot{z}_f + \dot{v}) & (15)\\
F_r = -k_r(-b\theta - z_r + v) - b_r(-b\dot{\theta} - \dot{z}_r + \dot{v}) & (16)
\end{cases}
$$

Taking the Laplace transform of Eqs. (17) – (19) and substituting the results into Eq. (9), the open-loop transfer function from cylinder velocity input to output height can be given in Eq. (20).

$$\ddot{\beta} = 0.0029421\dot{l}_c - 1.0995\ddot{l}_c + 1.958\beta + 97.014\theta - 10.053v + 1.5394\dot{\theta} - 0.21343\dot{\beta} \quad (17)$$

$$\ddot{\theta} = -0.0029421\dot{l}_c - 0.44167\ddot{l}_c - 1.958\beta - 97.014\theta + 10.053v - 1.5394\dot{\theta} + 0.21343\dot{\beta} \quad (18)$$

$$\ddot{v} = -0.10486\dot{l}_c - 0.1624\ddot{l}_c + 16.36\beta + 100.06\theta - 141.32v + 1.7672\dot{\theta} - 2.375\dot{\beta} \quad (19)$$

$$P_{com}(s) = L\left\{\frac{h(t)}{\dot{l}_c}\right\} = \frac{3.5832(s+1.48\pm12.9i)(s+1.05\pm11.7i)}{s(s+1.35\pm12.9i)(s+0.61\pm8.87i)} \quad (20)$$

B. Hydraulic Sub-System Modeling

As mentioned in II.A, an electro-hydraulic actuator is used to control the angle between the header and combine body. The dynamics in the electro-hydraulic system come primarily from the valve. The steady state valve flow is proportional to the current command I_{in} as given in Eq. (21). The flow dynamics are thereby dominated by the second order characteristics between the current command and the actual valve displacement given in Eq. (22) .

$$Q_{1,static} = K\sqrt{\Delta p}(I_{in}) \tag{21}$$

$$Q_{1,dynamic} = \frac{Q_{static}}{s^2 + 2\zeta_v \omega_v s + \omega_v^2} \tag{22}$$

where K is a flow coefficient, Δp is the pressure difference across the valve, ζ_v and ω_v are the damping ratio and natural frequency of the valve. For the experimental system, the valve bandwidth was validated as 10Hz.

If one assumes the pressure difference upstream and downstream of the valve is constant and the valve dynamics are sufficiently high bandwidth, the electro-hydraulic system can be simplified to be a cylinder velocity $\dot{l}_c$ proportional to the current command I_{in} with a time delay. As will be seen, the delay incorporates frictional effects [5] in the cylinder seals and linkage bearings. When the system is operating at different header positions, the time delay varies due to the kinematically dependent nonlinear characteristics of the friction in the mechanical system. Here, the delay is assumed to be constant. The hydraulic system dynamics can then be considered as given in Eq.(23), where k_{hydr} is the corresponding coefficient (Table I).

$$\dot{l}_c(t) = k_{hydr} I_{in}(t - T) \tag{23}$$

III. Model Validation

A. Hydraulic Sub-System Model Validation

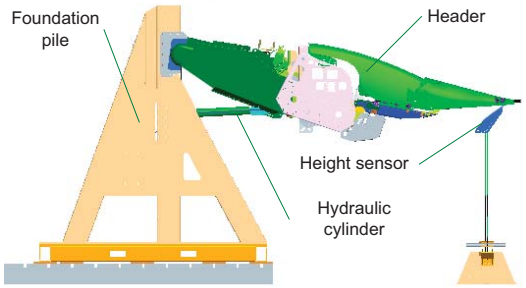

Fig. 5 Hydraulic system test bed

To validate the simplified electro-hydraulic system from Section II.B, the hydraulic actuation had to be separated from the combine. Fig. 5 illustrates a novel test stand designed to perform this task. The foundation pile acts as reaction wall for the actuator to push on with no pitch or heave dynamics as would be found on the actual combine. A header is also attached to provide a realistic inertial load for the actuator to move. The valve and pump systems are replicated from a production combine system and a height sensor is installed on the header tip to measure the header height. Additionally, several pressure sensors are installed throughout the hydraulic system for diagnostic purposes.

To measure the time domain response of the hydraulic system, a step command is applied to the control valve and the available signals are monitored as shown in Fig. 6. There is a combination of responses which include the time to open valves (t1), to stroke the load sensing pump (t2), to build up pressure of the pump output (t3), and to overcome system friction (t4). Summing these effects results in a total time delay $T = 0.3s$.

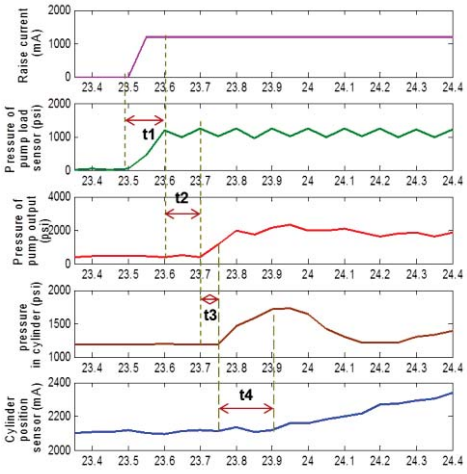

Fig. 6 Open loop step response of hydraulic system for input current

To verify that a pure time delay (Eq.(23)) represents the major characteristic of the hydraulic system, the closed loop step responses from simulation and experiment are compared in Fig. 7 . A proportional controller is used to make the header follow a step reference. In order to minimize chattering about a setpoint, a position dead zone is introduced with magnitude of 10 percent of the height range. The results of Fig. 7 indicate that the simulations results seem to match the response of the actual system sufficiently well so as to have confidence in the simplified model in Eq.(23).

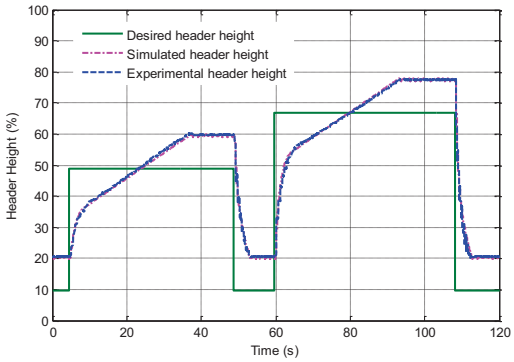

Fig. 7 Closed loop step response of the test system

B. Mechanical Sub-System Model Validation

The mechanical sub-systems experiments were performed on an experimental John Deere combine + header system shown in Fig. 8. For this validation it was not possible to introduce a perfect actuator and thereby separate the electro-hydraulic sub-system from the mechanical sub-system. However, given the validity of the electro-hydraulic sub-system demonstrated in III.A, the effect of actuation model error affecting the validation of the mechanical sub-system model is minimized. The mechanical sub-system model from Section II was validated by both frequency domain and time domain responses. For the frequency domain responses, a simple controller was utilized

to generate a closed-loop transfer function both in simulation and experimentally.

Fig. 8. Experimental combine used for field test results

A series of sinusoidal height references were fed to both closed loop systems under the conditions that the combine was on a level flat ground and not moving forward. The output heights were collected and compared with the reference signals. Performing a frequency by frequency analysis of magnitude and phase differences allowed for the construction of a Bode plot for both the simulation and experimental systems which can be compared in Fig. 9. It should be noted that the simulation system used was the nonlinear system given by Equations (1) – (16) rather than the linearized system of Eq. (20) demonstrating the accuracy of the nonlinear model. The model fits the physical system well in the magnitude plot. The phase plots have some differences, primarily due to the assumption of a constant friction level, and hence delay, in the hydraulic sub-system. In the experimental system, the friction varies with a change in relative orientation between the combine and header which is the primary cause of the phase differences.

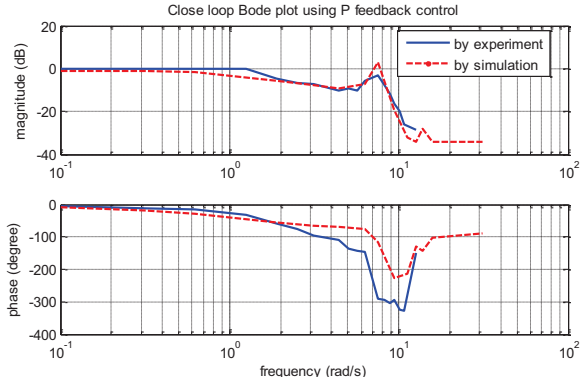

Fig. 9. Closed-loop bode plots comparisons between experimental results and simulation.

IV. Fundamental Limitations

A. Under-actuated and Non-collocated Systems

Under-actuated systems are those that possess fewer numbers of actuators than the number of degrees of freedom (DOFs). Assume an under-actuated manipulator has *n* independent DOFs, *m* of which are actuated, and the remaining *l=n-m* DOFs are called passive. As illustrated in [6], the corresponding *n* generalized coordinates can be written as $q^T = \left(q_1^T, q_2^T\right)$, where $q_1 \in R^l$ and $q_2 \in R^m$ corresponds to the passive DOFs and active DOFs respectively. The dynamic equations of the *n* DOF system can be written as [7]:

$$M_{11}\ddot{q}_1 + M_{12}\ddot{q}_2 + h_1 + \phi_1 = 0 \tag{24}$$

$$M_{21}\ddot{q}_1 + M_{22}\ddot{q}_2 + h_2 + \phi_2 = \tau \tag{25}$$

where the vector function $h_1\left(q,\dot{q}\right) \in R^l$ and $h_2\left(q,\dot{q}\right) \in R^m$ contain Coriolis and centrifugal terms (likely small in our application), the vector function $\phi_1\left(q\right) \in R^l$ and $\phi_2\left(q\right) \in R^m$ contain gravitational terms, and $\tau \in R^m$ represents the input generalized force.

Assuming inputs are forces and outputs are displacements, the transfer function from an input to an output always has an order of *2n,* which is determined by the natural frequencies of the *n* DOFs. The placement of the sensors will influence the zeros in the transfer functions as is shown in the following analysis. To make the analysis relevant to the case of the header height problem only a single input single output (SISO) system is considered.

For the case when the output is affected by both the active DOFs and passive DOFs, a coordinate transformation is used to generate the zeros dynamics. Assuming the output of the system is $y = Cq = \begin{pmatrix} C_1 & C_2 \end{pmatrix}\begin{pmatrix} q_1 \\ q_2 \end{pmatrix}$, where $|C_1| \neq 0$ and $|C_2| \neq 0$, the coordinates can be transformed as $\bar{q} = Tq$, where $\bar{q}^T = \left(q_1^T, \bar{q}_2^T\right)$ and $T = \begin{bmatrix} I_m & 0 \\ C_1 & C_2 \end{bmatrix}$. Since $|C_2| \neq 0$, the transform matrix T is nonsingular, and this coordinate transformation is valid. Following the same procedure as above, the original system is equivalent to Eq. (26) - Eq. (27) with internal dynamics of the system being represented by Eq. (26).

$$\left(M_{11} + M_{12}C_1\right)\ddot{q}_1 + h_1 + \phi_1 = -M_{12}C_2\upsilon \tag{26}$$

$$\ddot{\bar{q}}_2 = \upsilon \tag{27}$$

$$y = \bar{q}_2 \tag{28}$$

The number of transmission zeros is determined by the degrees of the internal dynamics. Therefore, for the system of Eq. (27) it equals to *2l*. Linearizing any nonlinearity associated with the manipulator dynamics, as done in Section II, results in a general transfer function for such an under-actuated system that can be written as Eq. (29).

$$P(s) = \frac{k\prod_{i=1}^{m}\left(s+z_i\right)\left(s+\bar{z}_i\right)}{\prod_{j=1}^{n}\left(s+p_j\right)\left(s+\bar{p}_j\right)} \tag{29}$$

Comparing the transfer function of Eq. (20) with the form in Eq. (29), it has an order of 5 instead of 6. The reason is the velocity input due to the nature of the flow control valves in the electro-hydraulic subsystem. If a pressure control valve set was used instead, the actuator input would be a force and

the transfer function in Eq. (20) would have an order of 6. For the combine system, the zero dynamics are highly influenced by the dynamics of the two passive DOFs as shown in Eq. (26).

B. Fundamental Limitations of Mechanical Sub-System

The actuator is installed between the header and combine body, the modes of the two passive DOFs are then excited and the low-frequency and lightly damped characteristic of the combine body dynamics (Fig. 3) is introduced into the system response. By Eq. (9), the output (h) is affected by all the three DOFs (β, θ, v) similar to the discussion previous to Eq. (26). As shown in Eq. (26), the internal dynamics of the combine and tire subsystem will then manifest as system zeros.

In the linearized combine system of Eq. (20), the four non trivial poles have undamped natural frequencies of 2.1 Hz and 1.4 Hz with corresponding damping ratios of 0.104 and 0.069, respectively. The non-collocated property induces low-frequency and lightly damped zeros, which have similar properties and values as the poles. The undamped natural frequencies of the zeros are 2.07 Hz and 1.87 Hz with the damping ratios as 0.114 and 0.0894. Such input/output pairs with low frequency and lightly damped zeros can limit the effects of feedback control [8] [9].

If we ignore the time delay in III.A and consider a simple proportional closed loop controller the open loop system behavior indicates difficulty in moving closed loop poles very far from their open loop location. This is due to the proximity between open loop poles and zeros as shown in Fig. 10. Two different values of $k_p = (0.284, 150.0)$ illustrate this fact.

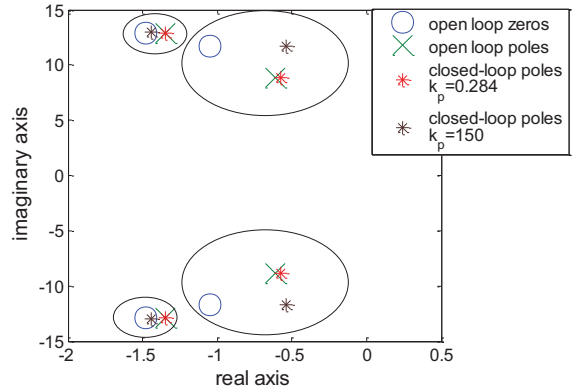

Fig. 10 Four closed-loop poles with respect to open loop poles and zeros

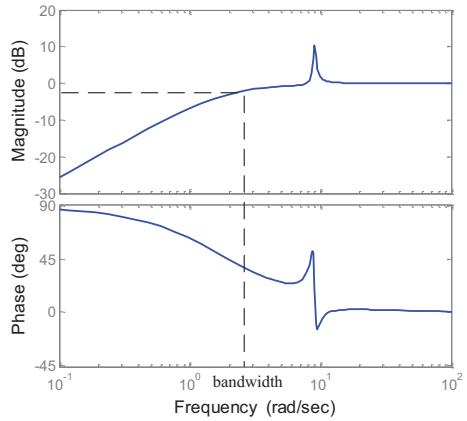

Fig. 11 Sensitivity functions using a P controller w/out delay

Fig. 11 gives the sensitivity function associated with $k_p = 0.284$. The closed loop system would not be able to reject ground disturbances occurring above approximately 0.4 Hz for this set of parameters. The peaks in the sensitivity function are due to the lightly damped closed loop poles resulting from the pairs of poles and open loop zeros shown in Fig. 10. Replacing the proportional C(s) by another controller may alter the shape of the sensitivity function in Fig. 11 somewhat but the Bode Sensitivity Integral [10] indicates that any reduction in the sensitivity function at lower frequencies would result in an increase, and hence possible instability due to lack of robustness, at higher frequency. Fundamentally, the performance is limited by the non-collocated and under-actuated nature of this system.

C. Time Delay Systems

It is well known that time delays in feedback systems reduce available bandwidth in order to maintain closed loop stability [11] [12]. Fig. 12 shows a sensitivity function of the system including the delay of 0.3 sec using a PI controller tuned to maximize bandwidth. With a delay, and correspondingly conservative gains, the bandwidth drops to 0.17 Hz.

$$k_{p1} = 0.1482 \quad k_{i1} = 0.018 \tag{30}$$

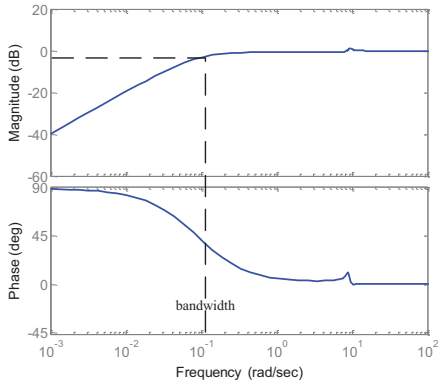

Fig. 12 Sensitivity functions using a PI controller w/delay

V. Simulation and Experimental Validation

The overall results in Section IV are very representative of the entire class of agricultural combines performing active header height control. The parameters may vary with combine and header sizes and more or less expensive electro-hydraulics resulting in quantitative variation from the results presented here. However the qualitative nature will remain. The mechanical sub-system is subject to under-actuation and non-collocation of sensing and actuation; the electro-hydraulic subsystem incurs a time delay in the input-put response. These are both combined in the overall system to severely limit achievable terrain disturbance rejection/tracking. This will now be demonstrated by examining performance tests for the experimental vehicle shown in Fig. 5.

A header tracking test is setup as shown Fig. 13. These tests were performed at a proving ground provided by an industrial partner. The combine is driven on level flat ground (concrete) between the test blocks and its wheels do not

encounter the blocks. The header attempts to track the profile of the trapezoidal blocks as the combine proceeds. Since the combine body does not incur the ground disturbances from the blocks the test isolates the performance of the header height closed loop tracking performance and does not confound it with a ground disturbance rejection test. Fig. 14 clearly shows that the phenomena described in Section II-IV are present and account for the level of performance achievable, and the responses in the black circle demonstrate that the performance of the system to track the test ground profile is unacceptable.

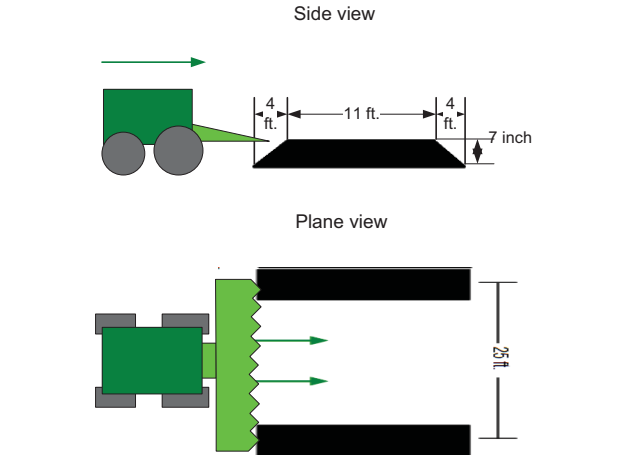

Fig. 13 Experimental test setup

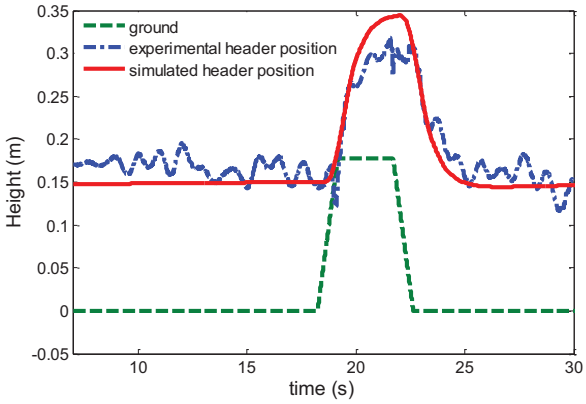

Fig. 14 Experiment verification

To specifically investigate the separate influences of the limitations described in Section IV we utilize the validated system and sub-system models in a simulated test environment. We utilize the same test shown in Fig. 14 and compare three cases: (1) the header is mounted on the test bed from Fig. 5 and travels between the test blocks with no actuator time delay (i.e. no combine dynamics); (2) the combine+header system tracks the test block profiles with no actuator time delay; (3) the combine+header system tracks the test block profiles with actuator delay. These 3 cases represent the system without any limitations, with only mechanical sub-system limitations, and with both mechanical and hydraulic limitations, respectively. In cases 1 and 2, the coefficients from Eq. (31) are used to maximize the performance, while in the case 3, the coefficients in Eq. (30) are used to ensure stability. Obviously, in case 1, without the limitations, a much more aggressive controller than the simple PI could be designed and implemented. However, we choose to maintain consistency here to quantitatively demonstrate the effects of the limitations.

$$k_{p2} = 0.1482 \quad k_{i2} = 1 \tag{31}$$

Fig. 15 illustrates the results of the 3 cases. When there are no limitations to the closed loop system (case 1) the header height can change rapidly to track the terrain shape. This would correspond to enabling high speed travel through the field and increased productivity. Unfortunately, when the mechanical sub-system limitation is introduced (case 2) the response of the system is reduced corresponding to the results of Section IV.A-IV.B. When both limitations are present (case 3), which is the case for the experimental combine system, the performance is even further deteriorated.

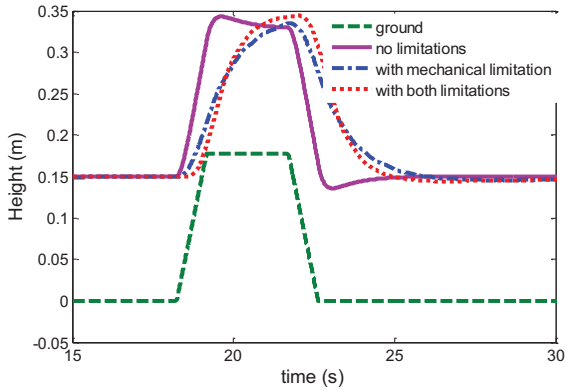

Fig. 15 Simulations for header ramp tracking which illustrate individual limitations

VI. Conclusion and Discussion

We used system dynamics and common analytical tools to gain insights into the fundamental limits for a combine harvester header height control system. Fig. 15 combined with the modeling and analysis of Sections II-IV, clearly demonstrate the challenges present in header height control and the reasons for the relative bottleneck in increasing vehicle speeds. The under-actuation and non-collocation properties of the mechanical system determine the position of the open-loop poles and zeros, which results in a system bandwidth upper limit. A time-delay limitation from the hydraulic actuator restricts the controller gains and further limits the achievable closed-loop performance.

Clearly, an improvement in the overall system performance cannot be achieved solely by feedback control design. Any improvements in the overall system performance would require a mechanical system redesign, an actuation system improvement, or possibly a utilization of additional information such as robust look-ahead sensing or predictive terrain maps. The ideal solution, from a performance consideration, would be some combination of these.

Acknowledgement

The authors appreciate the support of John Deere Company for this paper.

APPENDIX

TABLE I
NOMENCLATURE

Symbol		Value
I_{com}, I_h	the inertias of combine body and header with respect to the gravity center and point A separately	66000kg·m² 22000kg·m²
m_{com}, m_h	the masses of the combine body and the header	15000kg 5000kg
h_0	the original height of the A point	1.2m
k_f, k_r	the spring constant of front and rear tires	1303720N/m 1673600N/m
b_f, b_r	the spring constant of front and rear tires	22400kg/s 26300kg/s
a, b	the distance in x direction between front/rear wheel axis and gravity center of combine body	2m 1.3m
ζ_h, ζ_{cgh}, $\varphi_{t1}, \varphi_{t2}$	structural angle (refer to Fig. 3 and Fig. 4)	0.3rad, 0.1rad 0.3rad, 0.5rad
l_{t1}, l_{t2} l_{cgh}, l_{ins} l_h, l_f	structural length (refer to Fig. 3 and Fig. 4)	2.9m,3m 2m,0.8m 4.6m,1.7m
k_{hydr}	coefficient from valve current to the velocity of the cylinder	0.032m/s/A
x_{cgh}, z_{cgh}	the distances between the header gravity center and the point A in x and z directions	variable
x_A, z_A	the distances between the combine body gravity center and the point A in x and z directions	variable
F_f, F_r	the forces on the combine body at the front and rear tires	variable
F_{Ax}, F_{Az}	the forces at the point A in x and z directions	variable
F_l	the force from the hydraulic cylinder on the header and combine body	variable
β	the header angle with respect to x axis	variable
θ	the pitch displacement of combine body	variable
v	the vertical displacement of combine body	variable
h	the absolute header height	variable
l_c	the cylinder length	variable
α,ρ,φ,γ	refer to Fig. 3 and Fig. 4 for the geometric meaning of these terms	variable

TABLE II
VARIABLE VALUE AT THE EQUILIBRIUM POINT

Symbol	Value	Symbol	Value	Symbol	Value
α_{ss}	0.113rad	ρ_{ss}	0.5221rad	γ_{ss}	1.0359rad
φ_{ss}	-0.1002rad	$l_{c,ss}$	1.3259m	β_{ss}	0.3866rad
θ_{ss}	-0.0171rad	v_{ss}	-0.0941m	$x_{A,ss}$	2.5922m
$z_{A,ss}$	-0.7321m	$F_{Ax,ss}$	157540N	$F_{Az,ss}$	446850N
$F_{l,ss}$	158330N	$f_{f,ss}$	94660N	$f_{r,ss}$	81900N

REFERENCE

[1] J. L. Glancey, "Analysis of Header Loss from Pod Stripper Combines in Green Peas," *Journal of Agricultural Engineering Research*, vol. 68, pp. 1-10, 1997.

[2] T. L. Kaminski and G. C. Zoerb, "Automatic Header-Height Control for Grain Crops," *Transactions of the Amerian Society of Agricultural Engineers*, pp. 284-287, 1965.

[3] G. T. Lopes, P. S.G. Magalhases, and E. G.O. Nobrega, "Optimal Header Height Control System for Combine Harvesters," *Biosystems Engineering*, vol. 81, no. 3, pp. 261-272, 2002.

[4] Yangmin Xie, Andrew Alleyne, Ashley Greer, and Deneault Dustin, "Header Height Control of A Combine Harvester System," in *Proceeding of ASME DSCC Dynamic Systems and Control Conference*, Boston, 2010.

[5] H. Olsson, K. J. Aström, C. Canudas de Wit, M. Gäfvert, and P. Lischinsky, "Friction Models and Friction Compensation," *European Journal of Control*, vol. 4, pp. 176-795, Dec 1998.

[6] Hirohiko Arai and Susumu Tachi, "Position Control of a Manipulator with Passive Joints Using Dynamic Coupling," *IEEE Transitions on Robotics and Automation*, vol. 7, no. 4, Aug. 1991.

[7] M.W. Spong and M. Widyasaga, *Robot Dynamics and Control*. New York: John Wiley & Sons, Inc., 1989.

[8] K. J. Aström, "Limitaions on Control System Performance," *European Journal of Control*, vol. 6, no. 1, pp. 2-20, 2000.

[9] J. S. Freudenberg and D. P. Looze, *Frequency Domain Properties of Scalar and Multivariable Feedback Systems*. New York: Springer-Verlag, 1988.

[10] M. M. Seron, J. Braslavsky, and G. Goodwin, *Fundamental Limitations in Filtering and Control*. New York: Springer-Verlag, 1997.

[11] Sigurd Skogestad and Ian Postlethwaite, *Multivariable Feedback Control Analysis and Design*. West Sussex: John Wiley & Sons Ltd, 2005.

[12] B. Magya, C. Hos, and G. Stepanl, "Influence of Control Valve Delay and Dead Zone on the Stability of a Simple Hydraulic Positioning System," *Mathematical Problems in Engineering*, 2010.

[13] M.W. Spong, "Partical Feedback Linearization of Under-actutated Mechanical Systems," in *Proceedings of the IEEE/RSJ/GI International Conference*, 1994, pp. 314-321.

[14] J. Freudenberg and D. Looze, "Right half plane poles and zeros and design tradeoffs in feedback systems," *IEEE Trans. Automat. Contr.*, vol. AC-30, pp. 5555-565, 1985.

[15] J. Chen, L. Qiu, and O. Toker, "Limitations in maximal tracking accuracy," *IEEE Trans. Automat. Contr.*, vol. 45, pp. 326-331, Feb. 2000.